Geochemistry Geophysics Geosystems G3
AN ELECTRONIC JOURNAL OF THE EARTH SCIENCES
Published by AGU and the Geochemical Society

Article
Volume 8, Number 5
25 May 2007
Q05P22, doi:10.1029/2006GC001360
ISSN: 1525-2027

Click Here for Full Article

Comparison of Mg/Ca- and alkenone-based sea surface temperature estimates in the fresh water–influenced Gulf of Guinea, eastern equatorial Atlantic

Syee Weldeab
Forschungszentrum Ozeanränder, Universität Bremen, Leobenerstrasse, D-28359 Bremen, Germany

Now at IFM-GEOMAR Leibniz Institute for Marine Sciences, University of Kiel, Wischhofstrasse 1-3, D-24148 Kiel, Germany (sweldeab@ifm-geomar.de)

Ralph R. Schneider
Institut für Geowissenschaften, Universität Kiel, Ludewig-Meyn-Str. 10, D-24118 Kiel, Germany

Peter Müller
Forschungszentrum Ozeanränder, Universität Bremen, Leobenerstrasse, D-28359 Bremen, Germany

[1] This study presents a comparison of sea surface temperature (SST) estimates based on Mg/Ca ratios of *Globigerinoides ruber* and alkenone unsaturation index ($U^{K'}_{37}$) in core sediment recovered from the Gulf of Guinea, eastern equatorial Atlantic. Mg/Ca- and $U^{K'}_{37}$-based SST estimates yield fairly comparable results for the time interval 21,000–14,500 years and for the late Holocene. The early and middle Holocene, however, are largely characterized by a discrepant trend, with warm Mg/Ca and cold $U^{K'}_{37}$ based SST estimates. This discrepant SST trend is accompanied by low sea surface salinity estimates (high riverine runoff) and biogenic sediment, which is characterized by high biogenic opal content, low carbonate content, and relatively low alkenone concentration. We hypothesize that the discrepancy in the reconstructed SSTs during the middle and early Holocene presumably suggests a period of elevated riverine input of dissolved silica and dominantly siliceous phytoplankton bloom in a low saline and warm surface water, while alkenone producers were likely prevalent in a season of cold SST and low riverine silica input. This study suggests that changes in the local hydrography and nutrient input have strong influence on the $U^{K'}_{37}$-based SST estimate that may be unraveled by combining different SST proxies.

Components: 6113 words, 4 figures.

Keywords: Mg/Ca SST and alkenone SST; paleothermometry; paleosalinity; eastern equatorial Atlantic; riverine discharge; Gulf of Guinea.

Index Terms: 4825 Oceanography: Biological and Chemical: Geochemistry; 4875 Oceanography: Biological and Chemical: Trace elements (0489).

Received 5 May 2006; **Revised** 5 February 2007; **Accepted** 21 February 2007; **Published** 25 May 2007.

Copyright 2007 by the American Geophysical Union

Weldeab, S., R. R. Schneider, and P. Müller (2007), Comparison of Mg/Ca- and alkenone-based sea surface temperature estimates in the fresh water–influenced Gulf of Guinea, eastern equatorial Atlantic, *Geochem. Geophys. Geosyst.*, *8*, Q05P22, doi:10.1029/2006GC001360.

Theme: Development of the Foraminiferal Mg/Ca Proxy for Paleoceanography
Guest Editor: P. Martin

1. Introduction

[2] Paleo-sea surface temperature estimates based on molecular and trace element variation in marine phyto- and zoo-planktons are commonly applied SST proxies; as such, they are crucial tools in paleoceanographic research. Combined with foraminiferal oxygen isotope ratios, these SST proxies allow reconstruction of $\delta^{18}O$ of seawater (proxy for SSS) providing insights into the evaporation and precipitation, and fresh water discharge history that govern the ocean circulation and determine climate instability.

[3] However, like other proxies for paleo-environmental reconstruction, alkenone and Mg/Ca ratios are affected by diagenetic alteration and/or environmental factors other than SST that may hamper their comparability and reliability as SST proxies [*González et al.*, 2001; *Grimalt et al.*, 2000; *Harvey*, 2000; *Nürnberg et al.*, 1996; *Brown and Elderfield*, 1996; *Lea et al.*, 1999; *de Villiers*, 2003; *Conte et al.*, 2006]. For instance, preferential dissolution of Mg [*Brown and Elderfield*, 1996; *de Villiers*, 2003], alteration by Mg-rich post-depositional precipitates (Fe-Mn-oxides and Mn-carbonate), and incomplete removal of terrigenous materials [*Lea et al.*, 2005; *Pena et al.*, 2005; *Weldeab et al.*, 2006] constitute constraints for the application of Mg/Ca paleothermometry. With regard to alkenone paleo-thermometry, the influence of dissolved nutrient distribution, degradation processes, and lateral transport of fine grained materials are reported to bias SST estimates [*Volkman*, 2000; *Grimalt et al.*, 2000; *Sachs et al.*, 2000; *Prahl et al.*, 2003b; *Benthien and Müller*, 2000]. Variation of SST estimates related to paleo-environmental conditions that affect seasonality and water column depth of the planktic foraminiferal calcification and alkenone production may be unraveled by co-analyses of foraminiferal Mg/Ca ratios and the alkenone unsaturation index ($U^{K'}_{37}$).

[4] This study compares Mg/Ca- and $U^{K'}_{37}$-based SST reconstructions and their relationship with other environmental proxies. Particular emphasis is focused on the Holocene epoch when western African experienced several rapid climate instabilities [*Gasse*, 2000; *Nguetsop et al.*, 2004; *Salzmann et al.*, 2002; *Shanahan et al.*, 2006] that are thought to be related to SST changes in eastern equatorial Atlantic [*Weldeab et al.*, 2005].

2. Material and Methods

2.1. Study Area

[5] Sea surface circulation in the Gulf of Guinea is governed by the Guinea Current (GC) [*Peterson and Stramma*, 1991; *Verstraete*, 1992]. The Gulf of Guinea flows eastward along the coast of west-equatorial Africa (Figure 1). In boreal summer, the Gulf of Guinea has its greatest eastward advection, bringing cold and salty surface water into the Gulf of Guinea [*Richardson and Walsh*, 1989] (Figure 2). In boreal winter, the GC is weak and surface water in the Gulf of Guinea is relatively warm (Figure 2). Throughout the year, the wind field over the Gulf of Guinea is dominated by a weak SW wind (Figure 1). Seasonal coastal upwelling is restricted to a small area along the northern boundary of the Gulf of Guinea (Figure 1) [*Hardmann-Mountford and McGlade*, 2003; *Picaut*, 1983; *Verstraete*, 1992] which is not related to local wind field and surface current, but to a far field forcing in the western equatorial that leads to shoaling of the Equatorial Undercurrent [*Picaut*, 1983; *Verstraete*, 1992]. Sea-surface salinity variation at the core site is controlled by fresh-water discharge of the Sanaga and Niger Rivers, which drain an area of ~2,4 million km^2 with a mean annual discharge volume of ~200 km^3 into the eastern part of the Gulf of Guinea (Global Runoff Data Center, Koblenz, Germany, 2005, http://grdc.bafg.de). Lowest sea surface salinity develops in the Gulf of Guinea when time of relatively high riverine runoff coincides with weak surface current mixing. This may explains the delay between the time of highest fresh water input and the development of salinity minimum over the

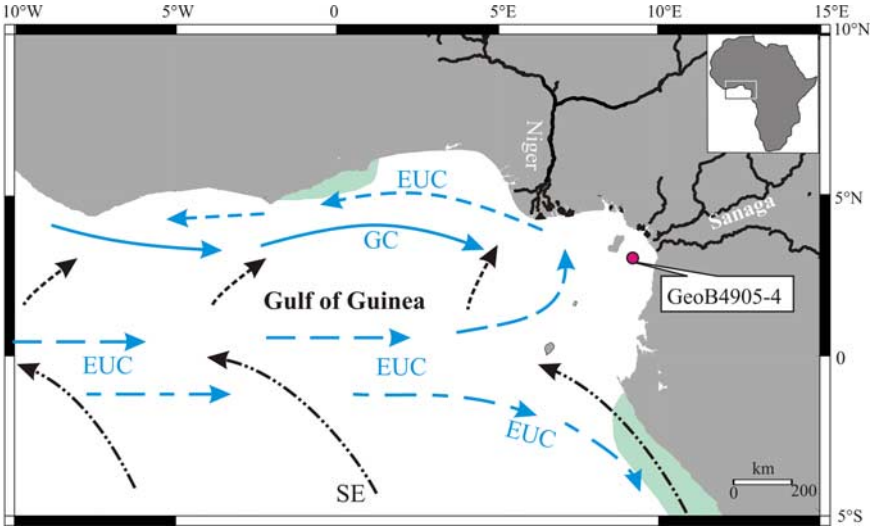

Figure 1. Map showing core location (2°30.0′N, 9°23.4′E, 1328 m), surface and subsurface currents, and wind field. Blue arrows and blue dotted arrows indicate the Guinea Current (CG) and the Equatorial Undercurrent (EUC), respectively. Black dotted arrows indicate southeastern trade winds (SE) that after crossing the equator change their direction toward northeast. Light green areas indicate areas of coastal upwelling; note that the upwelling along the northern boundary of Gulf of Guinea is not related by local wind or surface current, but is due to a seasonal change of the EUC in western tropical Atlantic, resulting in shoaling of the EUC as it flows westward along the northern boundary of the Gulf of Guinea [*Hardmann-Mountford and McGlade*, 2003; *Picaut*, 1983; *Verstraete*, 1992].

core site (Figure 2). A season of elevated riverine fresh water discharge lasts from August to November, reaching the highest discharge in October (Figure 2). At the core site, the average sea-surface salinity (SSS) at 0–20 m water depth [*Levitus*, 1994] continuously decreases from 31 practical salinity unit (psu) (August) to 27.5 psu (December), reflecting the peak of riverine discharge between mid-July and November (Figure 2). During periods of low riverine discharge (February–July), the SSS steadily increases from 28 psu (February) to 31.5 psu (July). Relatively warm sea surface temperature (SST) prevails from January to March (28.5 to 29.5°C). Starting in May, SST continuously declines, reaching the coldest value of 26°C in July August (Figure 2). Increasing concentrations of dissolved silica and chlorophyll-a over the core site [*Conkright et al.*, 2002] correlate with the start of the period of high riverine discharge, and remain high up to March (Figure 2). Dissolved phosphate and nitrate (not shown) are low throughout the year, ranging between 0.2 and 0.1 μM and 1 and 2 μM, respectively.

2.2. Sample Preparations

[6] Core GeoB4905-4 was recovered during Meteor Cruise M41/1 from the Gulf of Guinea in the

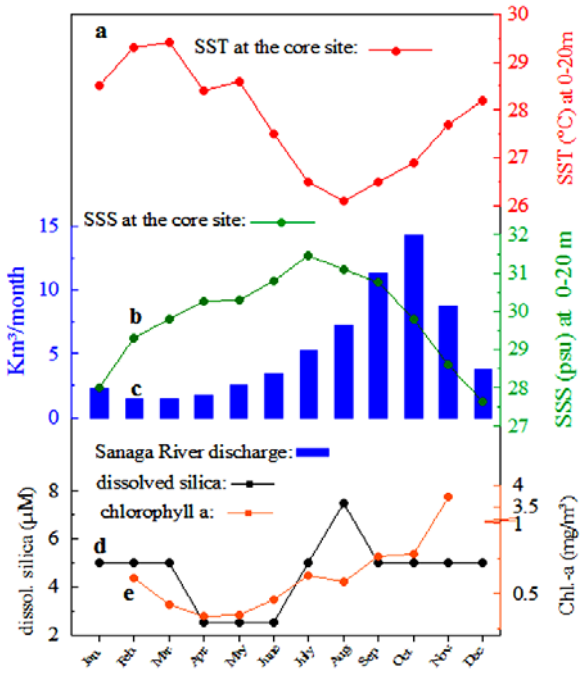

Figure 2. Monthly hydrographic conditions over the investigated core site: (a) sea surface temperature [*Levitus*, 1994], (b) sea surface salinity [*Levitus*, 1994], (c) riverine fresh water discharge of the Sanaga River (Global Runoff Data Center, Koblenz, Germany, 2005, http://grdc.bafg.de), (d) dissolved silica, and (e) chlorophyll-a concentration [*Conkright et al.*, 2002].

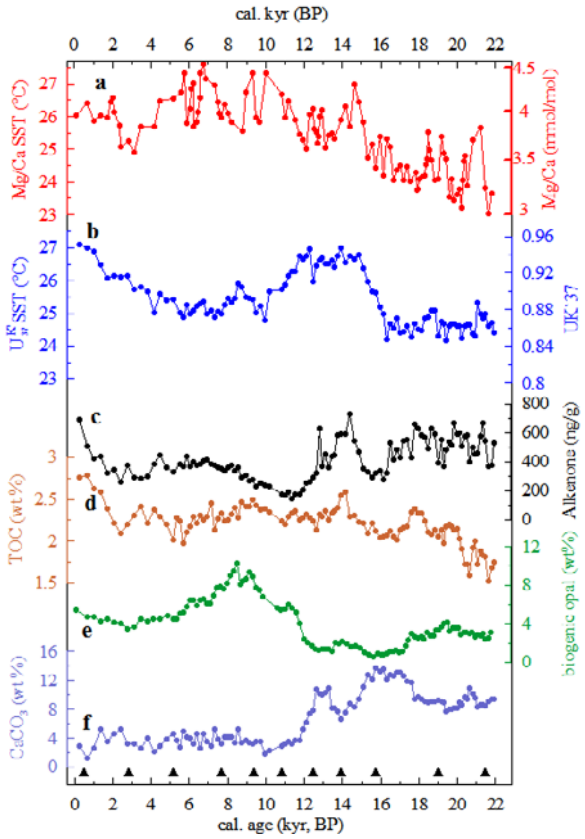

Figure 3. Geochemical parameters analyzed in GeoB4905-4 versus calibrated age (kyr, BP): (a) Mg/Ca ratios of *G. ruber* pink and Mg/Ca SST [*Weldeab et al.*, 2005], (b) $U^{K'}_{37}$ index and $U^{K'}_{37}$ index based SST, (c) total alkenone concentration, (d) total organic carbon (TOC) content, (e) biogenic opal content, and (f) carbonate content. The ^{14}C-AMS dated control points for the age model are indicated by triangles along the *x* axis.

eastern equatorial Atlantic (2°30.0′N, 9°23.4′E, 1328 m), ~115 km southwest of the mouth of the Sanaga River (Figure 1). The age model of core GeoB4905-4 is based on eleven ^{14}C-AMS datings of monospecific samples of *Globigerinoides ruber* pink and mixed planktonic foraminifers and the covers the last 21,000 calendar years (cal. kyr) [*Adegbie et al.*, 2003; *Weldeab et al.*, 2005]. Mg/Ca analysis was conducted on tests of *G. ruber* pink (250–300 μm), which reflects temperature of the uppermost 25 m of the water column [*Anand et al.*, 2003; *Deuser and Ross*, 1989; *Hemleben et al.*, 1989], and is published in a previous study [*Weldeab et al.*, 2005]. Details of the Mg/Ca cleaning procedure and measurement are described by *Weldeab et al.* [2005]. Briefly, approximately 60 individuals of *G. ruber* pink (250–300 μm) were gently crushed and transferred into acid-leached 0.5 ml-vials. Cleaning reagents included reductive and oxidative solutions. The Mg/Ca measurements were conducted by ICP-OES (Perkin Elmar Optima 3300 R). Standards and replicate analyses of samples gave a mean reproducibility of ±0.07 Mg/Ca mmol/mol. Fe/Ca and Mn/Ca ratios, which were collected at the same time as Mg/Ca, were used to monitor the cleaning results. Both Fe/Ca and Mn/Ca ratios vary between 0.05 and 0.3 mmol/mol and show no correlation with Mg/Ca ratios indicating no significant contribution of Mg associated with Fe- and Mn-phases. Mg/Ca SST was calculated using the calibration equation (Mg/Ca[mmol/mol] = 0.38exp(0.09*T[°C])) developed by *Anand et al.* [2003]. The standard error estimate, related to the translation of Mg/Ca to calcification temperature, accounts for ±1°C [*Anand et al.*, 2003].

[7] Sample preparation and extraction for $U^{K'}_{37}$ analyses were performed as described by *Müller et al.* [1998]. The extracts were analyzed by capillary gas chromatography using an HP 5890A gas chromatograph equipped with a 50 m 0.32 mm i. d. HP Ultra 1 fused silica column, split/splitless injection (1:10 split modus), and flame ionization detection. Helium was used as carrier gas. The oven temperature was programmed from 50 to 150°C at 30°C/min, from 150 to 230°C at 8°C/min, from 230 to 320°C at 6°C/min, and the final temperature maintained for 45 min. For the conversion of the $U^{K'}_{37}$ index to SST, we used the global surface water calibration [*Conte et al.*, 2006].

[8] Biogenic opal content was determined with the sequential leaching technique [*DeMaster*, 1981], modified by *Müller and Schneider* [1993]. $CaCO_3$ and total organic carbon (TOC) contents were determined as follows. Total inorganic carbon (TIC) was determined with an "Eltra C-S 500" C-S Analyzer by acid digestion followed by coulometric determination of the evolved CO_2, from which the $CaCO_3$ is coulometrically determined. Total carbon (TC) analyses with the C-S Analyzer were carried out by combustion at 1200°C, followed by coulometric determination of the evolved CO_2. The difference between TC and TIC was assumed to originate from the combustion of organic matter. The precision and accuracy were 0.1% and 0.2%, respectively.

3. Results

[9] During the time interval 21–16 kyr before present (BP) both Mg/Ca SSTs and $U^{K'}_{37}$ SSTs reveal relatively close co-variation (Figure 3). At

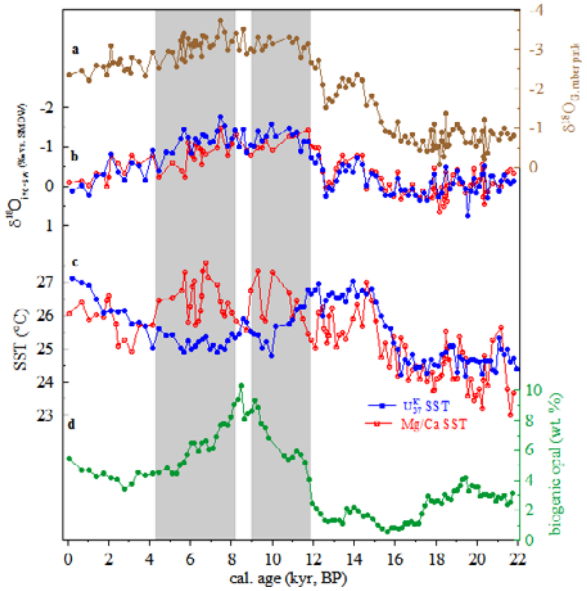

Figure 4. Surface water conditions during the last 21 kyr: (a) oxygen isotope composition of *G. ruber* pink ($\delta^{18}O_{G.\ ruber\ pink}$) [*Weldeab et al.*, 2005], (b) ice-volume corrected oxygen isotope composition of seawater ($\delta^{18}O_{ivc\text{-}sw}$) computed using $\delta^{18}O_{G.\ ruber\ pink}$ and $U^{K'}_{37}$ SST (blue line) and Mg/Ca SST (red line), (c) Mg/Ca SST [*Weldeab et al.*, 2005] and $U^{K'}_{37}$ SST, (d) biogenic opal content. Grey shaded areas indicates intervals of relatively low $\delta^{18}O_{ivc\text{-}sw}$ (low salinity), divergent SSTs record, and enhanced opal content.

around 16 cal. kyr, $U^{K'}_{37}$ SST starts to increase, reaching its highest value at around 14.7 kyr and remaining stable until 12 kyr BP. In contrast, gradual increase of Mg/Ca SST starts at ~18 kyr BP and shows significant short-term variability. In the time intervals of 12–9 and 8–4 kyr, Mg/Ca SST and $U^{K'}_{37}$ SST exhibit divergent evolution (Figures 3 and 4c). Mg/Ca SST shows a long-term warming and is punctuated by short term variability. Starting from ~6 kyr BP, gradual cooling is indicated by the Mg/Ca and at ~2.5 kyr BP reaches a value of 25°C. Afterward, Mg/Ca SST increases to 26.5°C and it remains in average stable. $U^{K'}_{37}$ SST indicates a cooling from ~12 to 9.5 kyr BP, a slight increase is documented between 9.3 and 8 kyr followed by a gradual increase from 7 cal. kyr to the present, reaching its highest value in the Holocene (Figure 3).

[10] During the time interval 21–12 kyr, carbonate, biogenic opal, TOC contents, and alkenone concentration vary between 7 and 13, 1 and 4, 1.7 and 2.5 wt.%, and 300 and 700 ng/g, respectively (Figures 3c–3f). Starting at around 12.25 kyr BP, pronounced change occurs in the biogenic component of sediment shown an increase of biogenic opal from 1 to 9 wt.%; and a decrease of carbonate content and alkenone concentration down to 4 wt.% and 200 ng/g, respectively. TOC contents show little variability, ranging between 2 and 2.5 wt.% throughout the time interval 14–2 kyr BP (Figure 3). Marked gradual increase of TOC content and alkenone concentration is documented starting at about 2 kyr BP.

[11] Variation of ice-volume corrected oxygen isotope composition of seawater ($\delta^{18}O_{ivc\text{-}sw}$), a proxy for sea surface salinity (SSS), has been extracted by subtracting temperature and continental ice volume effects on the $\delta^{18}O$ of *G. ruber* (pink) using temperature – $\delta^{18}O_{calcite}$ – $\delta^{18}O_{sw}$ relationship [*Bemis et al.*, 1998] and $\delta^{18}O$ estimates related to the variations of continental ice volume [*Waelbroeck et al.*, 2002]. The two curves of $\delta^{18}O_{ivc\text{-}sw}$ shown in Figure 4b were obtained using Mg/Ca SST and $U^{K'}_{37}$ SST to subtract the temperature effect on the $\delta^{18}O$ of *G. ruber*.

[12] Assuming 0.21‰ changes in the local $\delta^{18}O_{icv\text{-}sw}$ per 1°C change in the SST [*Bemis et al.*, 1998], the Holocene variation of Mg/Ca- and $U^{K'}_{37}$-based SST estimates (2.5–2°C) leads to changes in the local $\delta^{18}O_{icv\text{-}sw}$ of ~0.5 and 0.4 ‰, whereas the variation of the local $\delta^{18}O_{icv\text{-}sw}$ accounts for 2‰ (0.5–1.5‰). Therefore temperature-related changes in the $\delta^{18}O_{icv\text{-}sw}$ explain only ~25% of the total variation. This indicates a dominant control of fresh water input in determining the local $\delta^{18}O_{icv\text{-}sw}$. Thus, despite the discrepancy of the Mg/Ca- and the $U^{K'}_{37}$-based SST estimates, both local $\delta^{18}O_{icv\text{-}sw}$ estimates reveal similar patterns of trend and magnitude (Figure 4b).

[13] The effect of salinity on foraminiferal Mg/Ca ratios has been investigated in culture experiments [*Nürnberg et al.*, 1996; *Lea et al.*, 1999]. These experiments suggest a slight increase of foraminiferal Mg in response to anomalous salinity increase. Our study suggests that Mg/Ca SST increase is generally accompanied by a low local SSS, as independently demonstrated by the $\delta^{18}O_{icv\text{-}sw}$ extracted using $U^{K'}_{37}$-SST and $\delta^{18}O$ composition of *G. ruber* pink (Figure 4b). Thus we argue that the salinity effect on rising Mg/Ca SST is not significant. Close correlation of salinity with $U^{K'}_{37}$ index is indicated in the Atlantic [*Sikes and Sicre*, 2002]. The authors, however, concluded that salinity has no effect on $U^{K'}_{37}$ index, arguing that the salinity and $U^{K'}_{37}$ index correlation they observed in the Atlantic is an artifact due to strong correlation between

salinity and temperature. $U^{K'}_{37}$-base SST estimates using water column samples from low salinity areas of the equatorial Atlantic [*Conte et al.*, 2006] appear to clearly support the above conclusion [*Sikes and Sicre*, 2002].

[14] Early diagenesis constitutes a serious constraint to the application of foraminiferal Mg/Ca thermometry. Depending on water depth and corrosivity of water masses, preferential dissolution of foraminiferal Mg can occur and bias Mg/Ca SST reconstruction toward low SST [*de Villiers*, 2003; *Brown and Elderfield*, 1996]. Shell examination and shell weight variation for defined shell size are used to detect possible dissolution [*de Villiers*, 2003; *Elderfield et al.*, 2002] and incorporation of water depth correction into the calibration equation has been applied to correct for dissolution effects [*Dekens et al.*, 2002]. Syn-sedimentary and post-depositional formation/precipitation of Mg-rich phases (Mn-Fe oxides, Mn-carbonates and secondary calcium carbonates) on the foraminiferal shell can also bias Mg/Ca ratios toward anomalously high values and leads to an overestimation of reconstructed SST [*Pena et al.*, 2005; *Weldeab et al.*, 2006]. However, inclusion of a reductive step in the Mg/Ca cleaning procedure successfully removes contaminants such as Fe- and Mn-oxides and Mn-carbonates [*Pena et al.*, 2005; *Weldeab et al.*, 2006]. In this study, based on shell examination, we rule out significant Mg dissolution. Patterns and values of Mn/Ca and Fe/Ca ratios analyzed in conjunction with Mg/Ca are commonly used for monitoring possible contamination, and do not indicate significant Mg contribution from Mn-Fe-phases to the Mg/Ca ratios.

[15] Few studies suggest significant alteration of the $U^{K'}_{37}$ index as a result of degradation processes [*Hoefs et al.*, 1998; *Gong and Hollander*, 1999]. Several studies based on degradation experiments [*Teece et al.*, 1998], water column analyses [*Bentaleb et al.*, 1999], core top sediment analyses [*Madureira et al.*, 1995; *McCaffrey et al.*, 1990; *Prahl et al.*, 1989, 1993], and down core analyses [*Prahl et al.*, 2003a], indicate that early diagenetic alteration does not significantly affect the $U^{K'}_{37}$ index, although C_{37} alkenone concentrations significantly decrease [*Madureira et al.*, 1995; *McCaffrey et al.*, 1990; *Prahl et al.*, 1989]. However, a discussion about differential degradation of di- and triunsaturated alkenone and its effect on SST estimate, originally noted by *Rosell-Melé et al.* [1995], is revived by *Conte et al.* [2006].

[16] Lateral transport (strong surface and bottom currents, and down slope processes) of fine-grained materials has been reported to significantly bias alkenone-based SST estimate resulting in overestimate [*Sicre et al.*, 2005] or underestimate [*Benthien and Müller*, 2000] thermal condition of overlaying surface water. The core site of GeoB4905-4 is under the influence of the Gulf of Gulf of Guinea Current, Equatorial Undercurrent, and the North Atlantic Deep Water. The contribution of laterally transported material to the alkenone signature is difficult to assess within the scope of this study. Thus, while other processes are discussed as likely explanations for the reconstructed SST discrepancy, the role of laterally transported material in affecting the alkenone-based SST estimates cannot be fully excluded.

4. Discussion

[17] The focus of the discussion is the prominent features that stand out when the Mg/Ca and $U^{K'}_{37}$ SSTs are compared: (1) at 15–12 kyr (BP) when warm and stabile SST is suggested by the $U^{K'}_{37}$ SST, and Mg/Ca SST estimates indicate general warming trend with low amplitude and frequent variability; (2) at 12–9.5 kyr (BP), when a continuous decrease in the $U^{K'}_{37}$ SST is accompanied by a steady Mg/Ca SST increase; and (3) at 8–4.5 kyr (BP) when low $U^{K'}_{37}$ SST is paralleled by warm and variable Mg/Ca SST estimates. The SST differences (early middle Holocene and deglacial) are beyond analytical and methodological uncertainties, and are most likely related to environmental factors (other than SST) resulting in deviating SST signatures. It is conspicuous that during the Holocene marked discrepancy between Mg/Ca- and $U^{K'}_{37}$-based SST records coincides with phases of low $\delta^{18}O_{sw}$ (low local SSS) and with increased deposition of biogenic opal (Figures 3 and 4). For instance, pronounced low $\delta^{18}O_{ivc\text{-}sw}$ and increased biogenic opal from 12 to 9.5 kyr is paralleled by significant $U^{K'}_{37}$ SST cooling and Mg/Ca SST warming trend. In contrast, increasing $\delta^{18}O_{ivc\text{-}sw}$ (increasing SSS), decreasing opal content, and decreasing Mg/Ca SST are synchronous with increasing $U^{K'}_{37}$ SST for the interval covering approximately the last 7 kyrs.

[18] Comparison of both Mg/Ca- and alkenone-based SST estimates with regional climate records shows that the Mg/Ca SST record closely correlates to terrestrial records [*Gasse*, 2000, and refer-

ences therein], indicating warm and cold Mg/Ca SSTs that coincide with humid and arid conditions in the African monsoon belt, respectively [*Weldeab et al.*, 2005]. Furthermore, co-variation of warm (cold) Holocene Mg/Ca SST with high (low) lake level record from the Lake Bosumtwi [*Gasse*, 2000; *Shanahan et al.*, 2006; *Weldeab et al.*, 2005, Figure 2], located north of the Gulf of Guinea, indicates that the Mg/Ca SST is consistent with the regional climate records and is interpreted to reflect mixed layer temperature [*Weldeab et al.*, 2005]. If this correct, what does reflect the cold $U^{K'}_{37}$ SST estimates during early and middle Holocene?

[19] It is well documented by terrestrial records [*Gasse*, 2000; *Nguetsop et al.*, 2004; *Talbot and Johannessen*, 1992; *Shanahan et al.*, 2006] that equatorial western Africa experienced extremely wet climate conditions during the early and middle Holocene, suggesting that the southernmost position of the ITCZ was located north of its current position, i.e., north of the east-west trending coast of equatorial West Africa. Therefore it is less likely that during the middle and early Holocene major changes in wind direction and the development of coastal upwelling established in the eastern part of the Gulf of Guinea. This is clearly supported by the absence of upwelling indicators in the planktonic foraminiferal composition. Thus it is less likely that the deviation between the Mg/Ca SST and $U^{K'}_{37}$ SST records is associated with seasonal signals in response to an establishment of coastal upwelling.

[20] Result from sediment traps demonstrates [*Anand et al.*, 2003] that the foraminiferal calcification temperature (derived from Mg/Ca) and $\delta^{18}O$ show strong seasonal variability. However, in the absence of seasonal upwelling throughout the GeoB4905-4 record, as evidenced by the absence of upwelling indicators in the planktic foraminiferal composition (not shown), we assume that seasonal SST variation was moderate and did not strongly affect planktonic foraminiferal composition. Several studies reveal that availability and depth of dissolved nutrients [*Bentaleb et al.*, 1999; *Epstein et al.*, 1998], the depth of the thermocline [*Ternois et al.*, 1997; *Ohkouchi et al.*, 1999], and depth of chlorophyll maximum [*Prahl et al.*, 1993] are important in determining the depth at which alkenone production takes place. According to *Ohkouchi et al.* [1999], water depth of alkenone production can be as deep as 130–150 m. Although there is no sediment trap result available from the eastern part of the Gulf of Guinea, we assume that the seasonal variability in the riverine runoff and riverine nutrient input certainly affect the calcification depth and production depth of alkenone.

[21] Given that the marked SST difference (warm Mg/Ca SST and cold $U^{K'}_{37}$ SST) is recorded at times of low salinity (i.e., high runoff), pronounced increase of biogenic opal, and decrease of total alkenone concentration (Figures 3 and 4), we hypothesize that the cause of divergent trends in the alkenone index and Mg/Ca-based SST estimates might be related to seasonal changes in the amount of riverine dissolved nutrient input. High dissolved silica input would give rise to a bloom of dominantly siliceous phytoplankton (diatoms, silicoflagellates, and radiolarians) in the low saline and warm upper part of the photic zone, leading to a relatively low flux of alkenone producing haptophytic algae. Conversely, during seasons of low dissolved silica input, flux of alkenone producing haptophytic algae dominates. This suggested alternating dominance of siliceous and calcareous phytoplankton is consistent with results of a sediment trap study from the Arabian Sea [*Haake et al.*, 1993], which show increased biogenic opal and decreased carbonate (coccolithophorids and foraminifers) flux concordant with increase of dissolved silica in the mixed layer. In a down core study from the Gulf of California, *Sancetta* [1995] showed that a high percentage of diatom species correlates with very low abundance or absence of calcareous nanno-fossils. Likewise low percentages of the bloom indicating diatom species are accompanied by relatively high calcareous nanno-fossils. The relationship in the alternating abundance of opal-secreting plankton groups and calcareous nanno-phytoplankton is interpreted in terms of competitiveness, whereby the latter is more competitive when nutrients are limited [*Sancetta*, 1995, and references therein]. On the basis of the biogenic composition and in analogy to the above findings [*Haake et al.*, 1993; *Sancetta*, 1995], we suggest that sustained high fresh discharge and enhanced dissolved silica input might have induced a seasonal bloom of siliceous plankton at surface water, shifting the relative proportion of alkenone producing nanno-phytoplankton flux to a season of low SST and reduced riverine input of dissolved nutrient. The proposed hypothesis for the middle and early Holocene, however, is unable to explain the pattern of $U^{K'}_{37}$ SST estimates at ~12–14.5 kyr (BP), with warm and relatively stable $U^{K'}_{37}$ SST estimates. This is difficult to reconcile with the

regional climate reconstructions [*Gasse*, 2000; *Talbot and Johannessen*, 1992], and may be associated with laterally transported alkenones from warmer surface water, as recently documented in the southern Indian Ocean [*Sicre et al.*, 2005].

5. Summary and Conclusion

[22] We compared two widely applied proxies for paleo-sea surface temperature in single sediment core from the Gulf of Guinea (eastern equatorial Atlantic). Markedly discrepant results are evident at the time interval between 12 and 4 cal. kyr BP, with warm Mg/Ca SST and cold $U^{K'}_{37}$ SST estimates. This time interval also indicates drastic changes in the local hydrography, as suggested by low salinity estimated (high riverine runoff) and opal as the dominant component of the biogenic sediment. The absence of upwelling indicators in the planktonic foraminiferal composition suggests that the differences in the Mg/Ca SST and $U^{K'}_{37}$ SST estimates is not related to seasonal upwelling. The Mg/Ca-based SST estimate is compatible with regional climate records and modeling studies and reflect most likely mixed layer conditions.

[23] We hypothesize that seasonal changes in riverine nutrient input may have strong effect on $U^{K'}_{37}$-based SST estimates. Elevated input of dissolved silica at times of high riverine fresh water input may preferentially give rise to siliceous phytoplankton in the less saline and warm surface water, which likely shifts the relative abundance of alkenone producing haptophytic algae to a season of low SST and low riverine runoff.

Acknowledgments

[24] The authors would like to thank Carsten Rühlemann, Enno Schefuss, and Dorothy Pak for valuable discussions that improved an earlier version of the manuscript. We thank two anonymous reviewers, the associate editor (Pamela Martin), and the editor (Lauren Labeyrie) for their thoughtful reviews and comments. We also would like to thank M. Klan and H. Buschoff for analytical assistance and S. Medley for improving the English. S.W. has been supported by the Deutsche Forschungsgemeinschaft (WE2686/2-1).

References

Adegbie, A. T., R. Schneider, U. Röhl, and G. Wefer (2003), Glacial millennial-scale fluctuation in central African precipitation recorded in terrigenous sediment supply and fresh water signals offshore Cameroon, *Palaeogeogr. Palaeoclimatol. Palaeoecol.*, *197*, 323–333.

Anand, P., H. Elderfield, and M. H. Conte (2003), Calibration of Mg/Ca thermometry in planktonic foraminifera from a sediment trap time series, *Paleoceanography*, *18*(2), 1050, doi:10.1029/2002PA000846.

Bemis, B. E., H. Spero, J. Bijma, and D. W. Lea (1998), Reevaluation of oxygen isotope composition of planktonic foraminifera: Experimental results and revised paleotemperature equations, *Paleoceanography*, *13*, 150–160.

Bentaleb, I., J. O. Grimalt, F. Vidussi, J.-C. Marty, V. Martin, M. Denis, C. Hatté, and M. Fontugne (1999), The C_{37} alkenone record of seawater temperature during seasonal thermocline stratification, *Mar. Chem.*, *64*, 301–313.

Benthien, A., and P. J. Müller (2000), Anomalously low alkenone temperatures caused by lateral particle and sediment transport in the Malvinas Current region, western Argentine Basin, *Deep Sea Res., Part I*, *47*, 2369–2393.

Brown, S. J., and H. Elderfield (1996), Variations in Mg/Ca and Sr/Ca ratios of planktonic foraminifera caused by post-depositional dissolution: Evidence of shallow Mg-dependent dissolution, *Paleoceanography*, *11*, 543–551.

Conkright, M. E., et al. (2002), *World Ocean Atlas 2001: Objective Analyses, Data Statistics, and Figures*, CD-ROM documentation, U.S. Dep. of Comm., Washington, D. C.

Conte, M. H., M.-A. Sicre, C. Rühlemann, J. C. Weber, S. Schulte, D. Schulz-Bull, and T. Blanz (2006), Global temperature calibration of the alkenone unsaturation index ($U^{K'}_{37}$) in surface waters and comparison with surface sediments, *Geochem. Geophys. Geosyst.*, *7*, Q02005, doi:10.1029/2005GC001054.

Dekens, P. S., D. W. Lea, D. K. Pak, and H. J. Spero (2002), Core-top calibration of Mg/Ca in tropical foraminfera: Refining paleotemperature estimation, *Geochem. Geophys. Geosyst.*, *3*(4), 1022, doi:10.1029/2001GC000200.

DeMaster, D. J. (1981), The supply and accumulation of silica in the marine environment, *Geochim. Cosmochim. Acta*, *45*, 1715–1732.

Deuser, W. G., and E. H. Ross (1989), Seasonally abundant planktonic foraminifera of the Sargasso Sea: Succession, deep-water fluxes, isotopic compositions, and paleogeographic implications, *J. Foraminiferal Res.*, *19*, 268–293.

de Villiers, S. (2003), Dissolution effects on foraminiferal Mg/Ca records of sea surface temperature in the western equatorial Pacific, *Paleoceanography*, *18*(3), 1070, doi:10.1029/2002PA000802.

Elderfield, H., M. Vautravers, and M. Cooper (2002), The relationship between shell size and Mg/Ca, Sr/Ca, $\delta^{18}O$, and $\delta^{13}C$ of species of planktonic foraminifera, *Geochem. Geophys. Geosyst.*, *3*(8), 1052, doi:10.1029/2001GC000194.

Epstein, B. L., S. D'Hondt, J. G. Quinn, J. Zhang, and P. E. Hargraves (1998), An effect of dissolved nutrient concentration on alkenone-based temperature estimates, *Paleoceanography*, *13*, 122–126.

Gasse, F. (2000), Hydrological changes in the African tropics since the Last Glacial Maximum, *Quat. Sci. Rev.*, *19*, 189–211.

Gong, C., and D. J. Hollander (1999), Evidence for the differential degradation of alkenone under contrasting bottom water oxygen conditions: Implication for paleotemperature reconstruction, *Geochim. Cosmochim. Acta*, *63*, 405–411.

González, E. L., U. Riebesell, J. M. Hayes, and E. A. Laws (2001), Effects of biosynthesis and physiology on relative abundances and isotopic compositions of alkenones, *Geochem. Geophys. Geosyst.*, *2*(1), doi:10.1029/2000GC000052.

Grimalt, J. O., J. Rullkötter, M. Sicre, R. Summons, J. Farrington, H. R. Harvey, M. Goñi, and K. Sawada (2000), Modifications

of the C_{37} alkenone and alkenoate composition in the water column and sediment: Possible implications for sea surface temperature estimates in paleoceanography, *Geochem. Geophys. Geosyst.*, *1*(11), doi:10.1029/2000GC000053.

Haake, B., V. Ittekkot, T. Rixen, V. Ramaswamy, R. R. Nair, and W. B. Curry (1993), Seasonality and interannual variability of particle fluxes to the deep Arabian Sea, *Deep Sea Res., Part I*, *40*, 1323–1344.

Hardmann-Mountford, N. J., and J. M. McGlade (2003), Seasonal and interannual variability of oceanographic processes in the Gulf of Guinea: An investigation using AVHRR sea surface temperature data, *Int. J. Remote Sens.*, *24*, 3247–3268.

Harvey, H. R. (2000), Alteration processes of alkenones and related lipids in water columns and sediments, *Geochem. Geophys. Geosyst.*, *1*(8), doi:10.1029/2000GC000054.

Hemleben, C., M. Spindler, and O. R. Anderson (1989) *Modern Planktonic Foraminifera*, Springer, New York.

Hoefs, M. J. L., G. J. M. Versteegh, W. I. C. Rijpstra, J. W. Leeuw, and J. S. Sinninghe Damsté (1998), Postdepositional oxic degradation of alkenones: Implication for the measurement of paleo sea surface temperature, *Paleoceanography*, *13*, 42–49.

Lea, D. W., T. A. Mashiotta, and H. J. Spero (1999), Controls on magnesium and strontium uptake in planktonic foraminifera determined by live culturing, *Geochim. Cosmochim. Acta*, *63*, 2369–2379.

Lea, D. W., D. K. Pak, and G. Paradis (2005), Influence of volcanic shards on foraminiferal Mg/Ca in a core from the Galapagos region, *Geochem. Geophys. Geosyst.*, *6*, Q11P04, doi:10.1029/2005GC000970.

Levitus, S. (1994) *World Ocean Atlas 1994*, vol. 4, *Temperature*, U.S. Dep. of Comm., Washington, D. C.

Madureira, L. A. S., M. H. Conte, and G. Eglinton (1995), Early diagenesis of lipid biomarker compounds in North Atlantic sediments, *Paleoceanography*, *10*, 627–642.

McCaffrey, M. A., J. W. Farrington, and D. Repeta (1990), The organic geochemistry of Peru margin surface sediments, I, A comparison of C_{37} alkenone and historical El Nino records, *Geochim. Cosmochim. Acta*, *54*, 1671–1682.

Müller, P. J., and R. R. Schneider (1993), An automated leaching method for the determination of opal in sediments and particulate matter, *Deep Sea Res., Part I*, *40*, 425–444.

Müller, P. J., G. Kirst, G. Ruhland, I. von Storch, and A. Rosell-Mellé (1998), Calibration of the alkenone paleotemperature index UK' based on core-tops from the eastern South Atlantic and the global ocean (60°N–60°S), *Geochim. Cosmochim. Acta*, *62*, 1757–1772.

Nguetsop, V. F., S. Servant-Vildary, and M. Servant (2004), Late Holocene climate change in West Africa: A high resolution diatom record from equatorial Cameroon, *Quat. Sci. Rev.*, *23*, 591–609.

Nürnberg, D., J. Bijma, and C. Hemleben (1996), Assessing the reliability of magnesium in foraminiferal calcite as a proxy for water mass temperatures, *Geochim. Cosmochim. Acta*, *60*, 803–814.

Ohkouchi, N., K. Kawamura, H. Kawahata, and H. Okada (1999), Depth ranges of alkenone production in the central Pacific Ocean, *Global Biogechem. Cycles*, *13*, 695–704.

Pena, L. D., E. Calvo, I. Cacho, S. Eggins, and C. Pelejero (2005), Identification and removal of Mn-Mg-rich contaminant phases on foraminiferal tests: Implications for Mg/Ca past temperature reconstructions, *Geochem. Geophys. Geosyst.*, *6*, Q09P02, doi:10.1029/2005GC000930.

Peterson, R. G., and L. Stramma (1991), Upper-level circulation in the South Atlantic Ocean, *Prog. Oceanogr.*, *26*, 1–73.

Picaut, J. (1983), Propagation of the seasonal upwelling in the eastern equatorial Atlantic, *J. Phys. Oceanogr.*, *13*, 18–37.

Prahl, F. G., L. A. Muehlhausen, and M. Lyle (1989), An organic geochemical assessment of oceanographic conditions at MANOP Site C over the past 26,000 years, *Paleoceanography*, *4*, 495–510.

Prahl, F. G., R. B. Collier, J. Dymond, M. Lyle, and M. A. Sparrow (1993), A biomarker perspective on prymnesiophyte productivity in the northeast Pacific Ocean, *Deep Sea Res., Part I*, *40*, 2061–2076.

Prahl, F. G., G. L. Cowie, G. J. De Lange, and M. A. Sparrow (2003a), Selective organic matter preservation in "burn-down" turbidites on the Madeira Abyssal Plain, *Paleoceanography*, *18*(2), 1052, doi:10.1029/2002PA000853.

Prahl, F. G., M. A. Sparrow, and G. V. Wolfe (2003b), Physiological impacts on alkenone paleothermometry, *Paleoceanography*, *18*(2), 1025, doi:10.1029/2002PA000803.

Richardson, P. L., and D. Walsh (1989), Mapping climatological seasonal variation of surface currents in the tropical Atlantic using ship drift, *J. Geophys. Res.*, *91*, 10,537–10,550.

Rosell-Melé, A., G. Eglinton, U. Pflaumann, and M. Sarnthein (1995), Atlantic core-top calibration of the U^K_{37} index as a sea-surface palaeotemperature indicator, *Geochim. Cosmochim. Acta*, *59*, 3099–3107.

Sachs, J. P., R. R. Schneider, T. I. Eglinton, K. H. Freeman, G. Ganssen, J. F. McManus, and D. W. Oppo (2000), Alkenones as paleoceanographic proxies, *Geochem. Geophys. Geosyst.*, *1*(11), doi:10.1029/2000GC000059.

Salzmann, U., P. Hoelzmann, and I. Morczinek (2002), Late Quaternary climate and vegetation of the Sudanian Zone of northeastern Nigeria, *Quat. Res.*, *58*, 73–83.

Sancetta, C. (1995), Diatoms in the Gulf of California: Seasonal flux patterns and the sediment record for the last 15,000 years, *Paleoceanography*, *10*, 67–84.

Shanahan, T. M., J. T. Overpeck, C. W. Wheeler, J. W. Beck, J. W. Pigati, M. R. Talbot, C. A. Scholz, J. Peck, and J. W. King (2006), Paleoclimatic variations in West Africa from a record of late Pleistocene and Holocene lake level stands of Lake Bosumtwi, Ghana, *Palaeogeogr. Palaeoclimatol. Palaeoecol.*, *242*, 287–302.

Sicre, M. A., L. Labeyrie, U. Ezat, J. Duprat, J. L. Turon, S. Schmidt, E. Michel, and A. Mazaud (2005), Mid-latitude southern Indian Ocean response to Northern Hemisphere Heinrich events, *Earth Planet. Sci. Lett.*, *240*, 724–731.

Sikes, E. L., and M. Sicre (2002), Relationship of the tetra-unsaturated C_{37} alkenone to salinity and temperature: Implications for paleoproxy applications, *Geochem. Geophys. Geosyst.*, *3*(11), 1063, doi:10.1029/2002GC000345.

Talbot, M. R., and T. Johannessen (1992), A high resolution palaeoclimatic record for the last 27,500 years in tropical West Africa from the carbon and nitrogen isotopic composition of lacustrine organic matter, *Earth Planet. Sci. Lett.*, *110*, 23–37.

Teece, M. A., J. M. Getliff, J. W. Leftley, R. J. Parkers, and J. R. Maxwell (1998), Microbial degradation under oxi and unoxic conditions as a model of early diagenesis: Long chain alkadienes, alkenones and alkyl alkenoates, *Org. Geochem.*, *29*, 863–880.

Ternois, Y., M. A. Sicre, A. Boireau, M. H. Conte, and G. Eglinton (1997), Evaluation of long-chain alkenones as paleo-temperature indicators in the Mediterranean Sea, *Deep Sea Res., Part I*, *44*, 271–286.

Verstraete, J.-M. (1992), The seasonal upwellings in the Gulf of Guinea, *Prog. Oceanogr.*, *29*, 1–60.

Volkman, J. K. (2000), Ecological and environmental factors affecting alkenone distributions in seawater and sediments, *Geochem. Geophys. Geosyst.*, *1*(9), doi:10.1029/2000GC000061.

Waelbroeck, C., L. Labeyrie, E. Michel, J. McManus, K. Lambeck, E. Balbon, and M. Labracherie (2002), Sea-level and deep water temperature changes derived from benthic foraminifera isotopic records, *Quat. Sci. Res.*, *21*, 295–305.

Weldeab, S., R. R. Schneider, M. Kölling, and G. Wefer (2005), Holocene African droughts relate to east-equatorial Atlantic cooling, *Geology*, *33*, 981–984, doi:10.1130/G21874.1.

Weldeab, S., R. R. Schneider, and M. Kölling (2006), Comparison of foraminiferal cleaning procedures for Mg/Ca paleothermometry on core material deposited under varying terrigenous-input and bottom water conditions, *Geochem. Geophys. Geosyst.*, *7*, Q04P12, doi:10.1029/2005GC000990.